THE JOURNAL OF PHYSICAL CHEMISTRY C
A JOURNAL OF THE AMERICAN CHEMICAL SOCIETY

pubs.acs.org/JPCC

Article

# Strain in Catalysis: Rationalizing Material, Adsorbate, and Site Susceptibilities to Biaxial Lattice Strain

Cheng Zeng,[‡] Tuhina Adit Maark,[‡] and Andrew A. Peterson*

Cite This: *J. Phys. Chem. C* 2022, 126, 20892−20902

Read Online

ACCESS | Metrics & More | Article Recommendations | Supporting Information

**ABSTRACT:** The binding strengths of reaction intermediates on a surface are often the principal descriptors of the effectiveness of heterogeneous catalysts. Although strain is a well-known theoretical strategy to modify binding strengths, and experimental methods have been introduced to directly induce strain, there is comparatively little systematic understanding of the binding energy susceptibilities of different adsorbates, materials, and surface sites to strain. In this work, we employ electronic structure calculations to develop such a systematic understanding. We utilize density functional theory calculations with 10 simple reaction intermediates adsorbed on four binding sites of five metal fcc(111) surfaces under an in-plane biaxial strain of ±2.0%. The responsiveness to strain is quantified using a single parameter named strain susceptibility, which we define as the slope of the adsorption energy versus strain. Typical values for this slope are in the tens of meV per unit percent strain. Based on these calculations, several general trends are identified. First, the material susceptibility order is found to be (Au, Pt) > Pd > (Ag, Cu), which we show can be correlated with the relative changes in d-band widths with strain. Second, binding sites with a higher degree of coordination to the adsorbate tend to exhibit a higher strain susceptibility. Third, adsorbates having higher valency tend to exhibit larger susceptibilities, and among adsorbates having the same valency, N- and O-containing adsorbates exhibit similar susceptibilities, but both show higher susceptibilities than that of C-containing adsorbates. The resulting changes in binding energy are compared to the linear scaling relations of adsorption and are found not to follow the published slopes, but rather to scale more closely with coordination number. This analysis can help to make predictions of which reactions are likely to respond favorably to strain and which catalysts may exhibit enhanced activity. Finally, an eigenforce model is used to rationalize the strain trends. The model-predicted susceptibilities show decent agreement with values by electronic structure calculations, differing by a mean absolute error of 0.013 eV/% for a variety of adsorption systems.

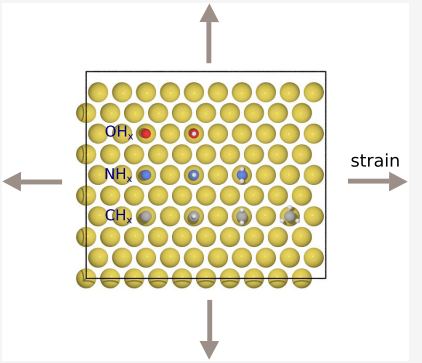




## 1. INTRODUCTION

Heterogeneous catalysts are the workhorses of industrial chemical transformations, and much effort is dedicated to enhancing the activity of such materials. Fundamentally, the bonding between the surface and reaction intermediates—including stable intermediates and transition states—dictates the elementary kinetics of a heterogeneous catalyst. A technique that is known for its ability to modify adsorption strengths, and thus tailor catalytic and electrocatalytic activity, is the application of strain. Pseudomorphic monolayer formation has been a widely implemented process as the inherent lattice mismatch between that of the deposited thin catalytic metal layer and the underlying substrate naturally brings about a strain effect.[1−6] It is now well accepted from electronic structure calculations that the tensile or compressive strain that the metal layer then feels leads to an upshift or a downshift, respectively, of its d-band.[7−10] The change in the d-band, often expressed as the shift of its central moment (d-band center, $\overline{\varepsilon}_d$), leads to differences in binding strengths. Such shifts ($\Delta\,\overline{\varepsilon}_d$) can also be estimated experimentally; for example, $\Delta\,\overline{\varepsilon}_d$ can be measured in terms of surface core-level shifts from X-ray photoelectron spectroscopy (XPS),[11−13] which can then be correlated to chemisorption energies.[14] Importantly, the changes in the electronic structure of the pseudomorphic overlayer relative to its bulk form are a result not just of the strain effect but also of the ligand effect arising from its interaction with the substrate.[10,15,16] Recently an eigenstress model derived from continuum mechanics by Khorshidi et al. provides an intuitive understanding of strain effect.[17] According to the model, the coupling between adsorbate-induced stress (eigenstress) and external strain determines the trend of binding energy change due to strain. The eigenstress model characterizes the strain effect in a qualitative manner. A quantitative analysis of strain effect can be achieved using an eigenforce model.[18] The eigenforce model has demonstrated

**Received:** October 14, 2022
**Revised:** November 15, 2022
**Published:** December 2, 2022

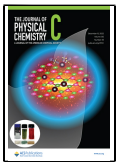




https://doi.org/10.1021/acs.jpcc.2c07246
*J. Phys. Chem. C* 2022, 126, 20892−20902

success in tuning Pt alloys for oxygen reduction reactions (ORR) by engineering anisotropic strains.[19]

Experimental efforts have been made to minimize the ligand effect, approaching a pure strain effect. Strasser et al.[13] used a dealloying technique on PtCu@Cu nanoparticles (NPs), resulting in a dealloyed Pt shell with a thickness of 0.6−1.0 nm; i.e., ≥3 monolayers were expected to be purely under a strain effect. The induced compressive strain resulted in an enhanced ORR activity. Sun et al.[20] showed that monodisperse Au/CuPt core/shell NPs exhibited enhanced catalytic activity for ORR and methanol oxidation relative to Pt NPs. As the thickness of the CuPt shell was large enough (1.5 nm), the ligand effect was presumed to be absent and the improved behavior was attributed to strain effects along with the alloying effect of Cu and Pt. Yang and co-workers demonstrated the effect of an externally applied uniaxial mechanical strain on the ORR activity of a PdCuSi metallic glass thin film.[14] The cyclic voltammetry shifts for the metallic glass from experiments and for Pd(111) surface from calculations due to strain were consistent in direction and magnitude and showed that compressive strain enhanced the ORR activity of the PdCuSi system while expansive strain suppressed it. Yan et al. used sputtered catalysts on a polymeric substrate, which could be directly strained in a mechanical testing device during the electrocatalytic hydrogen evolution, and showed strain effects to closely match theoretical predictions from electronic structure calculations—that is, compressive strain increases hydrogen evolution reaction (HER) activity of metals left to the volcano peak.[21] In another work by Yan et al., a similar procedure was applied to tungsten carbide that could lead to experimentally realizable strains up to 1.4%.[22] The work by Deng et al. demonstrated the effect of a cyclic elastic strain on Au and Pt electrodes with respect to the hydrogen evolution reaction (HER).[23] It was found that in agreement with the positions of the two metals on the HER volcano curve, the exchange current density of Au increased and of Pt decreased under tensile strain. Johnson et al. built a novel device that used static air pressure to allow direct strain tuning of nickel thin films in a high-temperature reactor, and the experimental design was tested on methanation reactions.[24] Tsvetkov et al.[25] have experimentally examined the effect of tensile, compressive, and no strain along the c-axis on the ORR kinetics of nanoscale $Nd_2NiO_{4+\delta}$ (NNO) thin films. The corresponding strain starts were obtained by depositing NNO on (111), (110), and (100) $Y_{0.008}Zr_{0.092}O_2$ (YSZ) single-crystal substrates. The ORR reactivity enhancement by tensile strain and reduction by compressive strain was correlated to the increase in the concentration of oxygen interstitials ($\delta$) and the better surface stability in the former case. The effect of strain engineering on oxides in particular has been discussed by Yildiz.[26] The author expounds that in these systems, the strain modifies both electrocatalysis and diffusion. This occurs by the induced changes of the oxygen defect formation energy, migration energy barrier, dissociation barrier, and charge transfer barrier in addition to the tuning of the adsorption energy.

Although many theoretical studies[10,18,27−31] have examined the effect of strain on the binding energies of specific catalytic intermediates, there has been little systematic description developed regarding the susceptibilities of differing materials, adsorption sites, and adsorbates to strain. In the present work, we report on our use of electronic structure calculations to develop such general guidelines, or rules of thumb, of the effect of strain categorized by material, adsorbate, and adsorption site, focusing on the case of in-plane biaxial strain. As many catalytic reactions are often limited by the linear scaling relations between adsorbates,[32−38] it is also an objective of this study to identify those cases for which deviations from scaling relations can be achieved by strain, which may lead to new catalytic possibilities. We also apply the mechanic eigenforce model to examine its effectiveness for diverse adsorption systems.

## 2. COMPUTATIONAL METHODS

In this work, electronic structure calculations were performed in density functional theory (DFT) with GPAW.[39,40] The Atomic Simulation Environment,[41] ASE, was used to perform the atomistic manipulations, including constructing cells and performing geometry optimizations. Both ASE and GPAW are open-source codes. The revised Perdew−Burke−Ernzerhof (RPBE) exchange−correlation functional of Hammer, Hansen, and Nørskov[42] was utilized because RPBE is specifically designed for adsorption processes, in particular for covalently bonded molecules.[42,43] No dispersion interactions were included as van der Waals interactions contribute little to adsorption energies for low-coverage strongly chemisorbed adsorbates studied in this work. The wavefunctions were expanded by plane wave bases with a cutoff energy of 450 eV for the ionic relaxation. Atomic positions were optimized using the quasi-Newton method, until the force on each atom was below 0.05 eV/Å. The one-electron Kohn−Sham states were occupied according to the Fermi−Dirac distribution with a smearing of $k_BT$ = 0.1 eV, and then the electronic energies were extrapolated to $k_BT$ = 0 eV. A dipole correction was added in the direction normal to the metal surfaces. No spin polarization was included in this work. Bulk lattice constants of Cu, Pd, Ag, Pt, and Au were calculated to be 3.69, 3.98, 4.20, 3.99, and 4.21 Å, respectively. Metal surfaces of Cu, Pd, Ag, Pt, and Au were modeled as 4 × 4 (surface atoms), simulating a low coverage of adsorbates. The unit cells were orthogonal periodic slabs in the fcc crystal structure with the fcc(111) facet exposed; simulations used a thickness of four layers and 20 Å of vacuum between slabs. For all surface calculations, we fix the bottom layer while allowing the top three layers to relax. A 3 × 3 × 1 Monkhorst−Pack $k$-point mesh was used to sample the Brillouin zone. To generate the strained M(111) surfaces, an in-plane uniform biaxial strain ($e_x = e_y$, denoted hereafter as $e_{x,y}$) within ±2% with a strain interval of 1% was applied by appropriately varying the optimized lattice vectors along the $x$ and $y$ directions. Since the atoms were unconstrained in the $z$ direction (except for the bottom fixed layer), the Poisson response normal to the surface is included automatically.

The adsorbates examined in the present study include the H atom and O-, N-, and C-centered H-containing molecular fragments, namely, $OH_x$ ($x$ = 0, 1), $NH_x$ ($x$ = 0−2), and $CH_x$ ($x$ = 0−3). The adsorption energies ($\Delta E$) for $OH_x$, $NH_x$, and $CH_x$ are reported using ($H_2$ and $H_2O$), ($H_2$ and $NH_3$), and ($H_2$ and $CH_4$), respectively, as reference energies $E^{ref}$. We adopt the convention that stronger binding is given by more negative numbers, that is, $\Delta E \equiv E[A^*] - E[^*] - E^{ref}[A]$, where the first two terms are the energies of the slab with and without the adsorbate present, respectively. Four binding sites were examined: the onefold ontop site, the twofold bridge site, and the threefold fcc and hcp sites. (The fcc site has no metal atom in the second atomic layer and the hcp site contains a



https://doi.org/10.1021/acs.jpcc.2c07246
J. Phys. Chem. C 2022, 126, 20892−20902

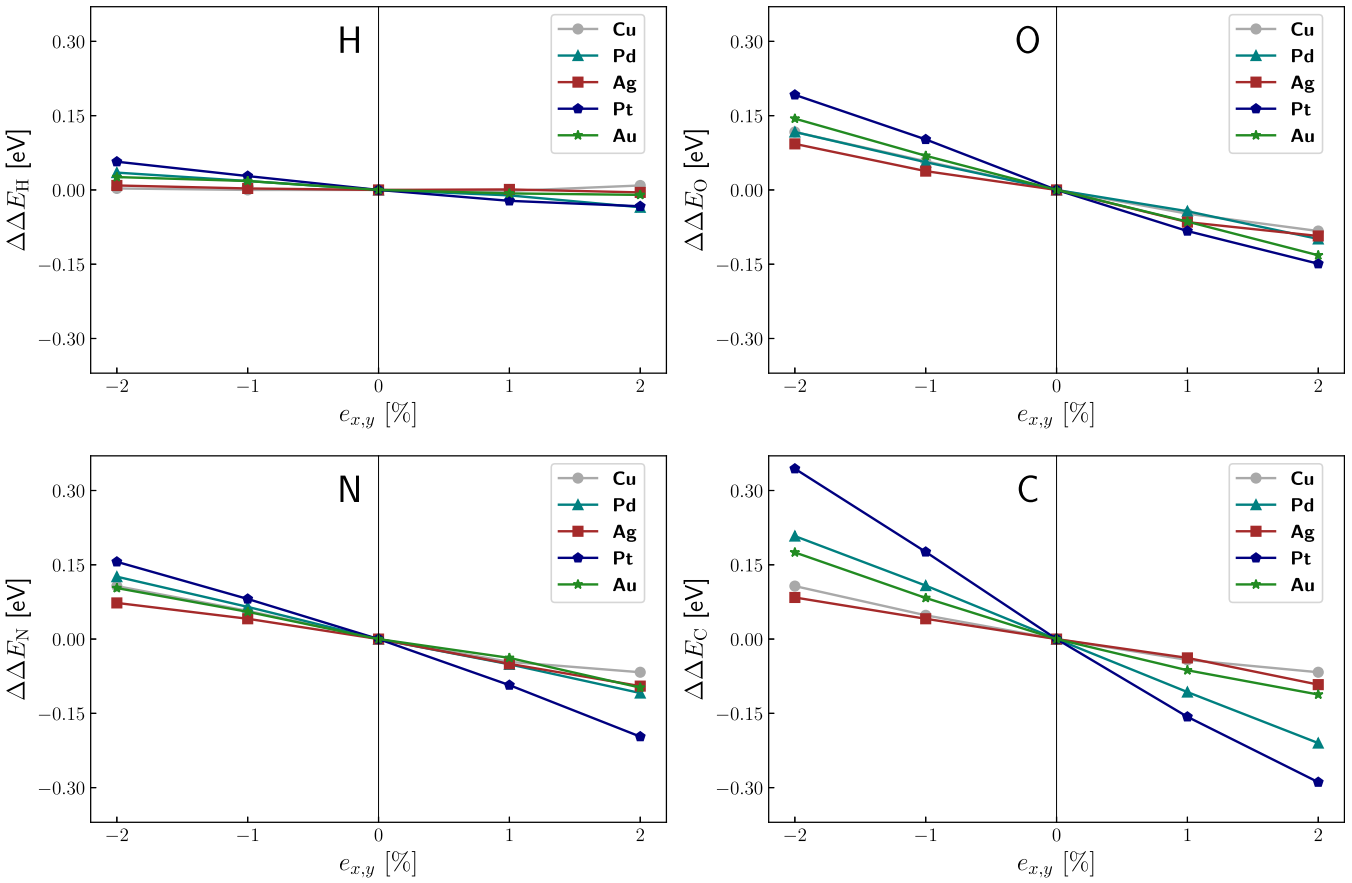


**Figure 1.** Variation of H, O, N, and C adsorption energies over fcc sites of Cu, Pd, Ag, Pt, and Au(111) surfaces as a function of in-plane uniform biaxial strain. For clarity, all adsorption energies are referenced to the corresponding strain-zero adsorption energies. Lines are a guide to the eye.

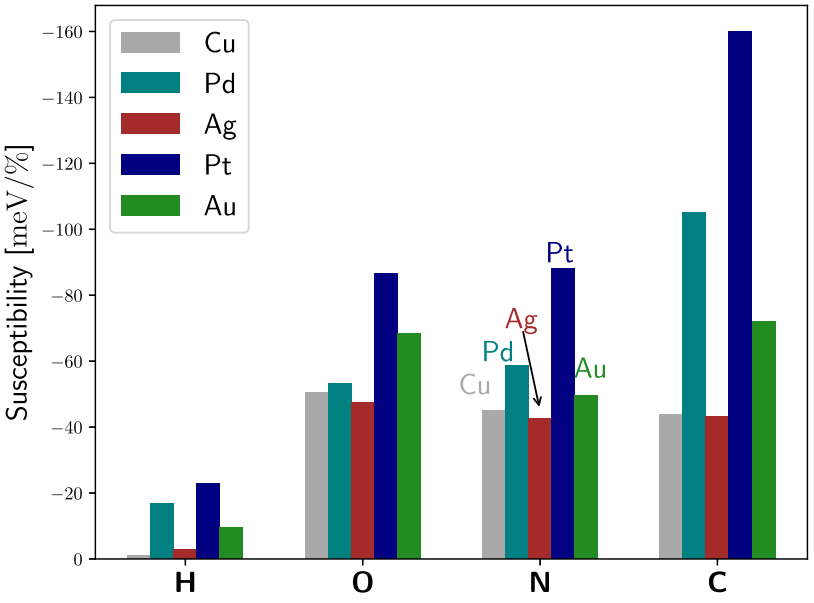


**Figure 2.** Strain susceptibility, quantified as slopes of the H, O, N, and C binding energy *vs.* strain plots in Figure 1 calculated between [−2:2]% strain.

metal atom directly below the site; oxygen tends to prefer the fcc site by 0.1−0.3 eV across many transition metals.[44]) To choose a set of adsorbate probes with which to examine the response of different metal (111) surfaces to strain, we first tested the adsorption energy variation of the atoms H, C, N, and O on the fcc site of metal surfaces involved. As will be presented later, when quantified by their susceptibilities ($d\Delta E/de_{x,y}$), H adsorption provided the weakest response while C provided the strongest, while O and N gave an intermediate response. Accordingly H, O, N and C were employed for deriving the material dependencies of strain to cover a range of probe responses.



https://doi.org/10.1021/acs.jpcc.2c07246
J. Phys. Chem. C 2022, 126, 20892−20902

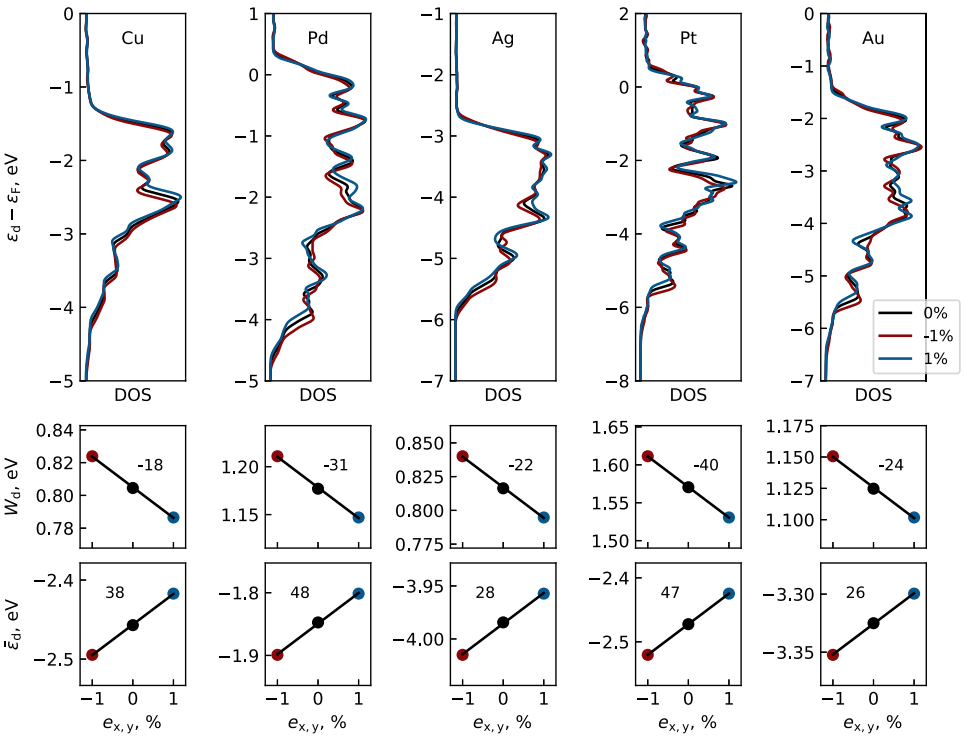


**Figure 3.** Response of the d-band electronic states to biaxial strain. The top row shows the d-orbital atom-projected density of states (DOS) on a surface atom of a clean fcc(111) surface of the specified metal allowed to relax in the direction orthogonal to the applied strain indicated in the legend. All d-orbital energies $\epsilon_d$ are reported with respect to the Fermi level $\epsilon_F$. The middle and bottom rows show the calculated width ($W_d$) and central moment ($\bar{\epsilon}_d$) calculated from the DOS distributions above. The slope ($dW_d/de_{x,y}$ or $d\,\bar{\epsilon}_d/de_{x,y}$) is reported in units of meV/(% strain) above each line.

The electronic structure calculations used to create the projected density of states figures were performed on a four-layer 2 × 2-atom orthogonal unit cell with 10 Å of vacuum between cells, and a dipole correction was employed. A $k$-point sampling of (8, 8, 1) was used with the RPBE exchange–correlation functional.

## 3. RESULTS AND DISCUSSION

**3.1. Material Dependencies.** In this section, we examine the susceptibility of different metals to biaxial strain, examining the metals Cu, Pd, Ag, Pt, and Au with the fcc(111) facet exposed. To characterize the strain response across this set of metal surfaces, we use a reduced set of probe adsorbates: H, O, N, and C. As described above, the choice is motivated by the high response of C and the low response of H binding energies to strain, relative to other adsorbates tested. To merely examine the material dependencies, the adsorbates were constrained to the threefold fcc site of the M(111) surfaces. Figure 1 displays the variation of H, O, N, and C binding energies ($\Delta E$) on this set of metals as a function of the applied in-plane uniform biaxial strain ($e_{x,y}$). Within this figure, we can broadly see the expected pattern that compression tends to weaken the binding, while expansion tends to strengthen it.

To simplify the data presentation, we report the slope ($d\Delta E/de_{x,y}$) in Figure 2; we refer to these values as the strain susceptibilities, denoted by $\chi_{strain}$. It is clear from the bar graph that irrespective of the adsorbate for these (111) surfaces, Au and Pt exhibit the strongest variation in adsorption energies with strain, while Cu and Ag show the least susceptibility to strain, with Pd laying intermediate.

To probe the electronic origins of materials' adsorption-strength susceptibility to strain, we conducted electronic structure calculations on adsorbate-free fcc(111) surfaces to examine how the d-band energy levels change with strain. Specifically, we applied biaxial strain of ±1% to periodic slabs and allowed for full relaxation in the direction orthogonal to the applied strain. The response of the electronic structure is shown in Figure 3.

The electronic response can be seen most clearly in the changes to the d-band density of states (DOS) for Cu. Here, we see that under tension (+1%) the DOS becomes more narrow, which is typically attributed to a reduction in the overlap in the d orbitals of adjacent atoms. Because the number of filling d electrons is unchanged, the fractional filling ($f$) of the d-band can be considered to be constant with strain perturbations; indeed, the largest change to the fractional filling that we observed with strain among the five metals studied in Figure 3 was less than 0.0016 for ±1% strain. Since the d-band is centered below the Fermi energy, to maintain a constant $f$, the d-band center ($\bar{\epsilon}_d$) must shift up, which can be seen to occur on the Cu DOS plot. With compression, we observe just the opposite effect.

Although subtle changes to the shapes of the distributions are observable for the remaining metals, the overall trends are the same as for Cu. This can be seen most clearly in the figures below each DOS, which show how $W_d$ and $\bar{\epsilon}_d$ change with applied strain. In these plots, we can see a systematic narrowing of the d-band with tension, accompanied by an upshift in the central moment. The slopes of the response ($dW_d/de_{x,y}$ or $d\,\bar{\epsilon}_d/de_{x,y}$) for each metal are shown above each line.



https://doi.org/10.1021/acs.jpcc.2c07246
J. Phys. Chem. C 2022, 126, 20892−20902

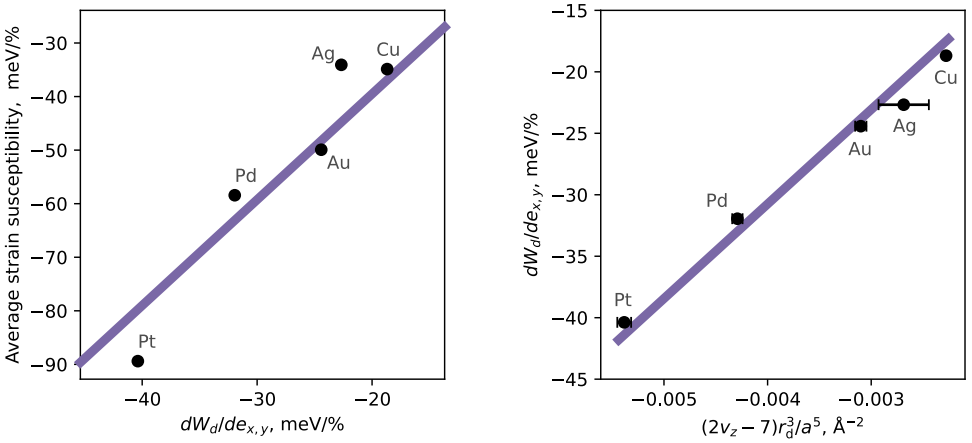


**Figure 4.** (Left) Correlation between the susceptibility of the d-band width to strain ($dW_d/de_{x,y}$) and the average strain susceptibility of all single-atom adsorbates involved at their most stable sites. The line is a best-fit proportionality, that is, linear regression with zero intercept. (Right) Correlation between the width susceptibility and the extent of d orbitals and interatomic distances, $(2\nu_z - 7)r_d^3/a^5$. The values of $r_d$ are taken from the Solid State Tables.[45] The line is also a best-fit proportionality. The horizontal error bars indicate the error of Poisson's ratios.

If we compare the strain susceptibility of the d-band width with the strain susceptibility of the average binding energies of four single-atom adsorbates at their most stable sites, we see a strong correlation for all metals: Pt has high susceptibilities on both metrics, while Cu and Ag have weak susceptibilities. This is shown in Figure 4, in which the average strain susceptibility is plotted versus the d-band width susceptibility. Overall we note that the adsorption energy changes with strain correlate much more strongly with the d-band width susceptibility than with the d-band center susceptibility; this can be traced to a weak correlation between the $dW_d/de_{x,y}$ and $d\,\bar{\varepsilon}_d/de_{x,y}$ (see Figure S1 in the SI), which may in turn be due to the low density of states near the Fermi level for some metals. Next, we will focus on how strain can be related to the change of d-band width.

The tight-binding model is a standard approach to understand the formation of the d-band in transition metals.[15,45,46] According to the tight-binding model, the d-band width of a surface atom $i$ is proportional to the interatomic matrix element between the d orbitals. The d−d orbital coupling matrix element reads as

$$V_i = \frac{\eta_{ddm}\hbar^2}{m}\sum_{j=1}^{NN}\frac{[r_d^{(i)}r_d^{(j)}]^{3/2}}{d_{ij}^5}$$

where $m$ is the mass of an electron, $r_d^{(i)}$ is the spatial extent of the d orbitals of that metal, $\hbar$ is the reduced Planck constant, $d_{ij}$ is the interatomic distance between atom $i$ and atom $j$, "NN" indicates that only interactions between nearest neighbors of atom $i$ are included, and $\eta_{ddm}$ is a dimensionless constant dependent on the type of d−d orbital interaction. The strain effect enters the denominator by changing the interatomic distance. For simplicity, $\eta_{ddm}$ is set as unity for all surfaces. With algebraic manipulation detailed in the Supporting Information, we find the derivative of the d-band width with respect to strain, $dW_d/de_{x,y}$, to be proportional to $(2\nu_z - 7)r_d^3/a^5$, where $a$ is the bulk lattice constant and $\nu_z$ is the Poisson's ratio in the $z$ axis when we apply an in-plane equi-biaxial strain. The values of $r_d$ are retrieved from the Solid State Table of Harrison.[45] When we plot the change in the d-band width versus $(2\nu_z - 7)r_d^3/a^5$, as shown in Figure 4(right), we see that this proportionality holds very well. Here, we can see that Pt and Pd, with their large extended d orbitals and small interatomic distance, have larger susceptibilities to changes in the d-band width (and, by correlation, to adsorption energies), compared to metals like Cu and Ag that have less extended d orbitals and thus smaller susceptibilities. This rationalizes the differences we see in the strain susceptibility of binding energies among these metals and provides a first-order expectation that this behavior may be more universal. Although five late-transition metals were chosen in this study, we expect the conclusions to be general among transition metals.

**3.2. Site Dependencies.** To understand how the type of adsorption site drives the adsorption energy response to biaxial strain, the adsorption of $OH_x$ ($x$ = 0, 1), $NH_x$ ($x$ = 0−2), and $CH_x$ ($x$ = 0−3) was considered on three fcc(111) adsorption sites (i.e., ontop, bridge, and hcp) for biaxially strained surfaces. Figure 5 shows the strain susceptibility plotted as a function of the coordination number of the adsorption site for this variety of adsorbates and surfaces. (When no data is shown for a particular configuration, it is because that adsorbate does not bind stably at that site.) A strong trend can be observed with coordination number: in general, the higher the coordination number of the adsorption site, the stronger the susceptibility to strain. This makes intuitive sense—for example, on the twofold sites, we need to consider the d−d orbital coupling matrix element with two surface atoms instead of one for ontop site adsorption. Therefore, the strain susceptibility of binding energies for a twofold site is larger because of the corresponding larger d−d orbital coupling matrix element. Alternatively, we can simply explain the higher susceptibility for a site with a larger coordination number by considering the more significant bond geometry changes. Nevertheless, a few cases show trends against the above conclusion, such as OH on Cu and O on Pt. We applied an eigenforce analysis to understand the unexpected trends for an example system (O on Pt). The eigenforce model is introduced and discussed in a subsequent section. The eigenforces on the most impactful surface atoms for both sites are shown in Figure S2. As a first-order approximation, we use only the largest eigenforces to compare the susceptibilities on the two sites. Let the shortest distance between two surface atoms be $a_0$, the biaxial strain be $\varepsilon$, the largest in-plane eigenforce be $F^{\ddagger}$, the number of surface atoms with the largest


https://doi.org/10.1021/acs.jpcc.2c07246
J. Phys. Chem. C 2022, 126, 20892−20902

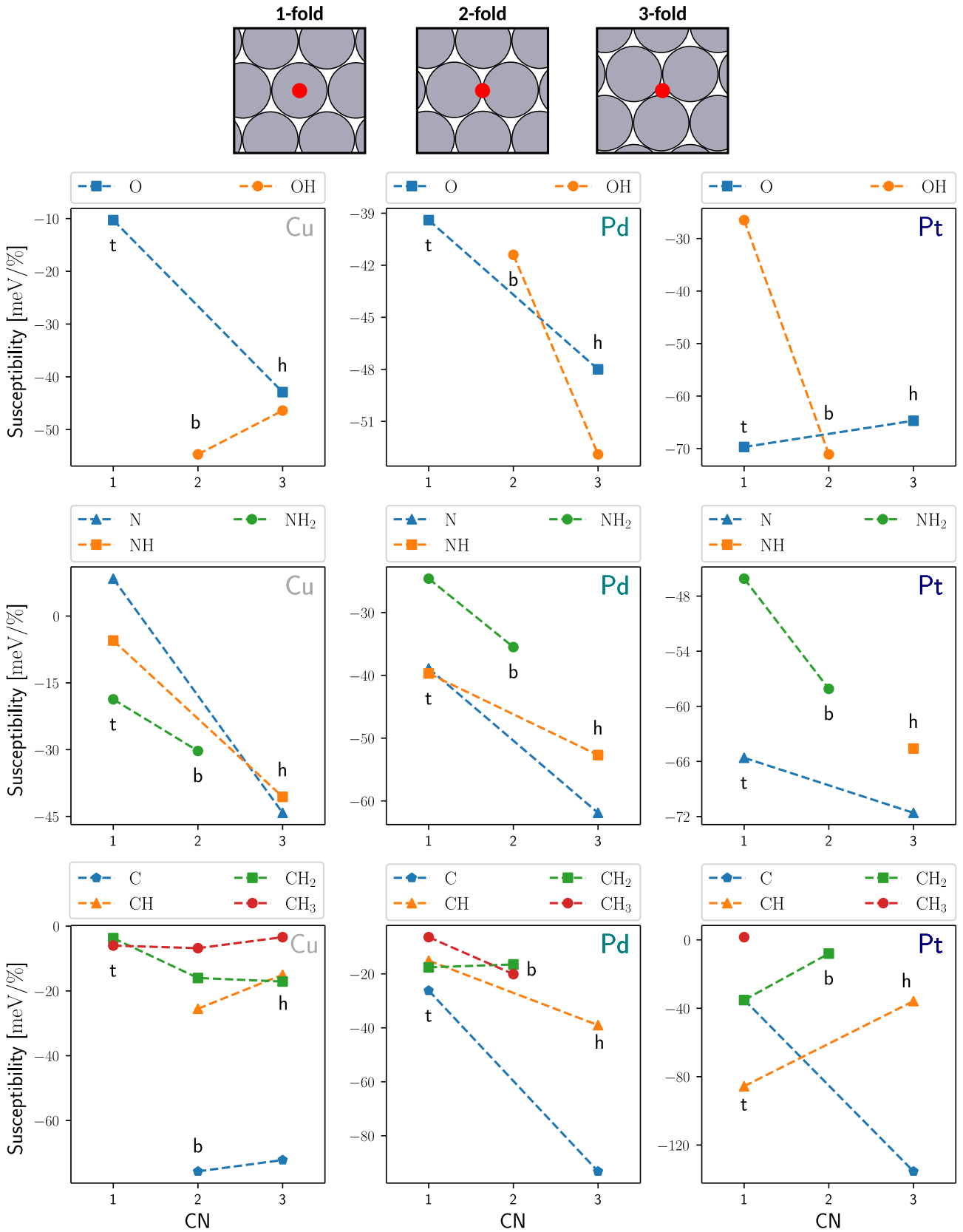


**Figure 5.** Strain susceptibility as a function of adsorption site coordination number. $OH_x$ ($x$ = 0, 1), $NH_x$ ($x$ = 0–2), and $CH_x$ ($x$ = 0–3) adsorption is considered on ontop (t), bridge (b), and hcp (h) sites. Dashed lines are a guide to the eye.

eigenforce be n, and the in-plane distance between adsorbate and the interested surface atoms be $l_0$. Therefore, for an ontop adsorption, we have $l_0 = a_0$, $n = 6$, and $F^{\ddagger} = 0.33$ eV/Å. For a hcp adsorption, we have $l_0 = a_0/\sqrt{3}$, $n = 3$, and $F^{\ddagger} = 0.64$ eV/Å. The strain-induced binding energy change is thus



https://doi.org/10.1021/acs.jpcc.2c07246
J. Phys. Chem. C 2022, 126, 20892−20902

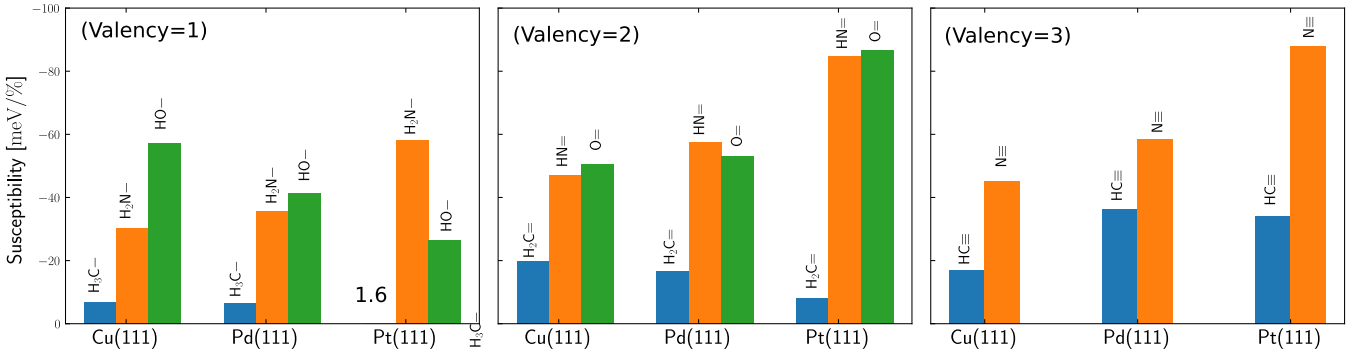


**Figure 6.** Strain susceptibilities for adsorbates having the same valency. Each adsorbate is at its most favorable site in the corresponding unstrained surface.

**Table 1. Susceptibilities in Units of meV/% between [−2:2]% Strain of Variation of Adsorption Energies of $AH_x$ and A with Strain and Slopes (Dimensionless) of Variation of Adsorption Energy of $AH_x$ vs A from the Present Work of ±2.0% Biaxially Strained Cu, Pd, and Pt(111) and the Latter Also for Unstrained M(111) Surfaces and Retrieved from Ref 32[a]**

| | Cu(111) | | | Pd(111) | | | Pt(111) | | | $AH_x$ vs A |
|---|---|---|---|---|---|---|---|---|---|---|
| relation | $AH_x$ | A | $AH_x$ vs A | $AH_x$ | A | $AH_x$ vs A | $AH_x$ | A | $AH_x$ vs A | (ref 32) |
| OH vs O | −57.2 | −50.6 | 1.13 | −41.4 | −53.1 | 0.78 | −26.5 | −86.7 | 0.31 | 0.50 |
| NH vs N | −47.1 | −45.1 | 1.04 | −57.5 | −58.6 | 0.98 | −84.8 | −88.0 | 0.96 | 0.71 |
| $NH_2$ vs N | −30.3 | −45.1 | 0.67 | −35.5 | −58.6 | 0.61 | −58.1 | −88.0 | 0.66 | 0.41 |
| CH vs C | −17.0 | −43.8 | 0.39 | −36.4 | −105.1 | 0.35 | −34.2 | −159.9 | 0.21 | 0.76 |
| $CH_2$ vs C | −19.7 | −43.8 | 0.45 | −16.5 | −105.1 | 0.16 | −8.0 | −159.9 | 0.05 | 0.49 |
| $CH_3$ vs C | −6.8 | −43.8 | 0.16 | −6.4 | −105.1 | 0.06 | 1.6 | −159.9 | −0.01 | 0.26 |

[a]Each adsorbate is adsorbed at its most favored site in the corresponding unstrained surface.

$$\Delta E_b(\varepsilon) = F^{\ddagger}\varepsilon l_0 n \quad (1)$$

The resultant susceptibility is given by $\chi = F^{\ddagger} l_0 n$. Plugging eigenforces and geometric parameters for both sites into the susceptibility formula, we can show $\chi_{ontop} > \chi_{hcp}$, as found in Figure 5.

**3.3. Adsorbate Dependencies.** To examine the effect of the chemical identity, e.g., C-, O-, or N-centered adsorbates, we first considered adsorbates that have the same valency. We defined the valency of an adsorbate $AH_x$ following Abild-Pedersen et al.,[32] as $x_{max} - x$, where the central atom can bond to a maximum of $x_{max}$ H atoms (e.g., the valency of CH is 3, and it can be represented as HC≡.) To mitigate any site effects in this analysis, we positioned all of the adsorbates at their most favorable sites. The susceptibilities to strain for the above adsorbates are shown in Figure 6. We can see the general trend that, irrespective of the valency, C-centered adsorbates are the least responsive to strain, while O- and N-centered adsorbates respond similarly to one another, with O-centered adsorbates tending to be slightly more susceptible. The susceptibility order of C < N ≈ O is probably related to the electronegativity order in Pauling scale, with C (2.55) < N (3.04) < O (3.44).[47,48] It is likely that a larger electronegativity difference between the adsorbate and metal implies a larger susceptibility, which however requires detailed investigation regarding the strain-induced changes of surface states and corresponding interactions with adsorbates.[49,50]

The effect of valency is also apparent from this data set. For consistency, we consider valency changes within a series of adsorbates that have the same central atom (e.g., 3, 2, 1 for HC≡, $H_2C$ =, and $H_3C$−). We found that mostly A atoms, which have the highest valency in a given set, respond more to strain than the $AH_x$ molecules ($x > 0$). However, the response order of N≡ and HN= was found to be different on different metals although the most preferred sites for both on all surfaces were fcc sites. A comparison of the $CH_x$ ($x$ = 0−3) series on Cu, Pd, and Pt showed that the trend was very clear: CH (valency = 3) > $CH_2$ (valency = 2) > $CH_3$ (valency = 1). Thus, we see a weak trend that higher valency adsorbates are more susceptible to strain.

**3.4. Linear Scaling Relationships.** Perhaps the most significant insight in recent catalysis theory is the development of the "scaling relations", formalized by Abild-Pedersen et al.,[32] which have led to a more systematic understanding of heterogeneous catalyst reactivity. These relations link the adsorption energies of, for example, $CH_x$ adsorbates to those of C adsorbates across surfaces in a linear manner. The scaling constant $\gamma$ was found to be a simple function of $x$: $\gamma(x) = (x_{max} - x)/x_{max}$, where $x_{max} - x$ is the valency, as described in Section 3.3. Similar relations were shown for central atoms other than C, including O, N, and S. Such scaling relationships have revolutionized our understanding of catalysis, but also put apparent limits on the improvement of catalysts as adsorption energies of key intermediates are inherently linked by these correlations.[51] It is an interesting question whether the changes in binding energies associated with the application of biaxial strain can cause deviations from these scaling relations. To examine this, in Table 1 for each pair of $AH_x$ and A (A = O, N, and C), we list the values for (a) susceptibilities of binding energy versus strain variation for the involved entities and (b) slopes of binding energy of $AH_x$ versus binding energy of A variation over the biaxially strained Cu, Pd, and Pt(111) surfaces. Additionally, the scaling constants relating each $AH_x$ and A pair binding energies over a variety of unstrained M(111) surface as taken from ref 32 are also provided. Each binding energy corresponds to the most preferred adsorption


https://doi.org/10.1021/acs.jpcc.2c07246
J. Phys. Chem. C 2022, 126, 20892−20902

site over the surface under consideration, as in the work by Abild-Pedersen et al.—so $AH_x$ and A are not necessarily adsorbed at the same position. If the slope of $AH_x$ vs A is close to the corresponding scaling constant, the strain effect will not result in a deviation from the scaling relationship and vice versa.

Some deviations from the scaling relations are suggested in Table 1. We can understand these deviations in the context of our previous analyses, taking the scaling between O and OH as an example. The slope of this scaling relation from the literature[32] is 0.5; however, slopes of 1.13, 0.78, and 0.31 are observed for Cu, Pd, and Pt, respectively. In all three of these metals, O atoms are found to adsorb most favorably on the fcc site. OH, however, binds at different sites on each metal: on Cu at an fcc site in a vertical orientation, on Pd at a bridge site in an angular orientation, and on Pt at the ontop site in an angular orientation. Recall from Section 3.2 that an fcc site responds more to strain than a bridge site, which in turn responds more than an ontop site. We can use this binding-site variability to explain the observations: the calculated linear scaling constant under strain is much greater for Cu, greater for Pd, and less for Pt than the value (0.5) for a series of unstrained metal (111) surfaces.

In the case of N, NH, and $NH_2$, adsorption takes place vertically on an fcc, fcc, and bridge site for all surfaces, respectively. Due to the site and adsorbate dependencies, in general, the response of NH and N binding energies to strain is more than that of $NH_2$. But among NH and N, the response of NH to strain is stronger than that of N on Cu, as reflected by the $\Delta E_{NH_x}$ vs strain susceptibility values in Table 1. Overall, slopes of the NH vs N and $NH_2$ vs N binding energy variation under strain are much larger than the respective known scaling constants 0.71 and 0.41.

Among the $CH_x$ adsorbate series, C and CH both bind to fcc sites on all of the three metals. $CH_3$ on Cu tends to adsorb on an fcc site, while on Au and Pt, it favors ontop sites. $CH_2$ on Cu prefers an fcc site, but on Au and Pt, it sits over a bridge site. Due to the site dependencies, the slopes of $CH_2$ vs C (0.45) and $CH_3$ vs C (0.16) on Cu are close to known constants of 0.49 and 0.26, respectively, while on Pt, significant departures from the linear scaling relationships are observed. In fact, a deviation to the scaling constant is also obvious for the CH vs C pair on Pt in that the responsiveness to the strain of C on Pt is strong, while that of $CH_x$ is relatively much weaker.

To visualize the deviation from the linear scaling relationships on application of strain, in Figure 7 we have showcased the $\Delta E_{NH_x}$ vs $\Delta E_N$ variation over strained Cu, Pd, Ag, Pt, and Au. From both Table 1 and Figure 7, it can be seen the slopes of $NH_x$ vs N under strain show a departure, in the same manner, from the linear scaling relationships. The strain-induced slopes of NH vs N are all close to 1, whereas the slopes of $NH_2$ vs N are around 0.66 excluding the case of Au. It follows a simple logic based on the site preference of the adsorbate pairs. The site coordination numbers for $NH_2$, NH, and N on all surfaces are 2, 3, and 3, respectively. In that sense, the slopes of susceptibilities can be estimated by the slopes of site coordination numbers, leading to predictions of 2/3 for $NH_2$ vs N, and 3/3 for NH vs N. Interestingly, this intuitive trend is also observed for OH vs O. Although the quantitative feature does not hold for $CH_x$ vs C pairs, it is qualitatively testable that $CH_x$ adsorbed on sites with high coordination numbers exhibit larger slopes of susceptibilities. It suggests a unique and perhaps general scaling relationship for strain itself, mainly due to the site dependencies of susceptibilities to strain. Results for scaling relations of OH vs O and $CH_x$ vs C are shown in Figure S3 and Figure S4 in the SI. We are careful to note that while the slopes may offer a path off of the constraints of the scaling relations, in reality, the magnitude of deviation away from the scaling lines is limited, as is shown for the case of high ±2% strains shown in Figure 7. However, we might expect that this will lead to strain having unique influences over catalytic activity for catalytic reactions in which the adsorbates studied herein are important, such as methane dehydrogenation, ammonia synthesis, and the oxygen reduction reaction.

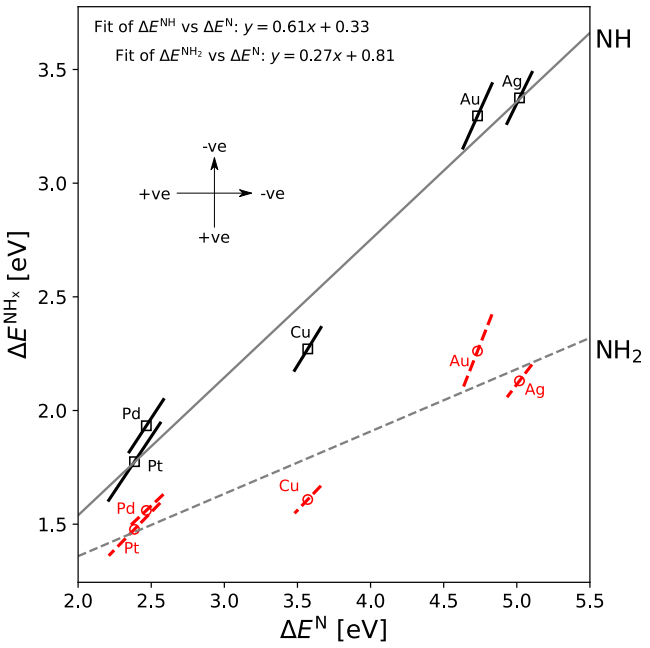


**Figure 7.** $\Delta E^{NH_x}$ vs $\Delta E^{N}$ variation for ±2.0% biaxially strained Cu, Pd, Ag, Pt, and Au(111) surfaces and the slopes or linear scaling constants fitted using the results without strain depicted as gray lines. The data points corresponding to pair adsorbates of ($NH_2$, N), and (NH, N) are represented by red circles and black squares, respectively. The strain-induced changes for ($NH_2$, N), and (NH, N) are plotted by red dashed and black solid lines, respectively. The arrows give the sign and direction of applied biaxial strain.

**3.5. Simplified Eigenforce Model to Describe the Strain Effect.** It is widely acknowledged that the d-band model provides a reliable route to describe the strain-induced binding energy change for adsorption on late-transition metals.[7,27] It justifies the strain effect across various metal surfaces for the same adsorbate with a similar adsorption configuration. However, exceptions to the strain predictions of a simple d-band model have been reported.[17] A more detailed description of electronic structure changes upon adsorption may be necessary to elucidate the deviations from the d-band model predictions.[52−54] In this section, a mechanic eigenforce model is used to describe pure strain effect on the binding change for a variety of adsorbate−surface-site combinations. The eigenforce model is adapted from the eigenstress model, introduced by Khorshidi et al.,[17] in which the binding energy change due to an external strain is described by the interaction energy between the adsorbate-induced stresses and the external strain. Since in atomistic systems strain/stress fields


https://doi.org/10.1021/acs.jpcc.2c07246
J. Phys. Chem. C 2022, 126, 20892−20902

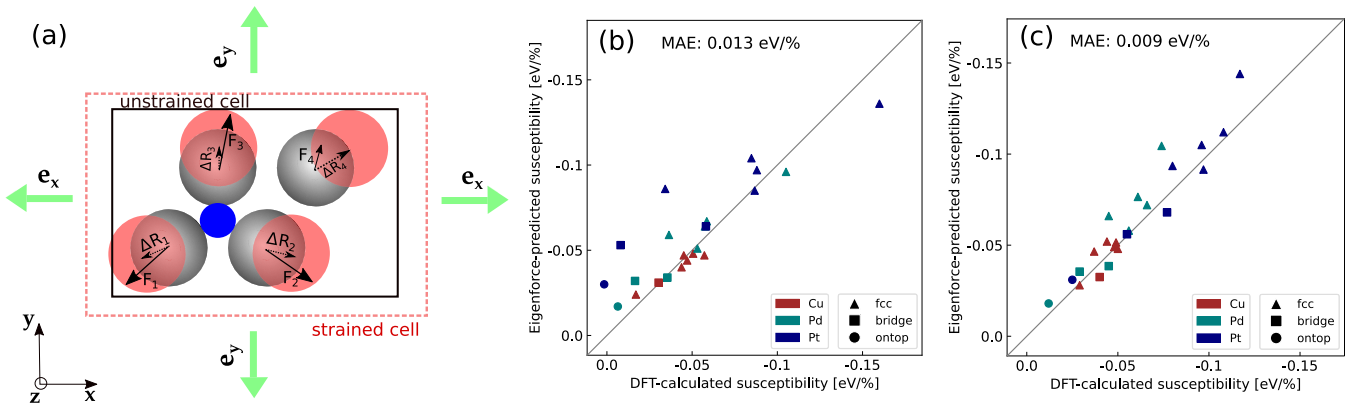


**Figure 8.** Eigenforce model-predicted strain susceptibilities. (a) Schematic illustration of the eigenforce model. (b) Eigenforce-predicted susceptibilities versus DFT-calculated values for fully relaxed systems. (c) Eigenforce-predicted susceptibilities versus DFT-calculated values for rigid systems. Marker colors and shapes represent respective surfaces and adsorption sites. More details of the comparisons are shown in Figures S5 and S6 in the SI, in the form of three separate plots for each metal surface.

are not well defined, a more realistic approach is to use forces and displacements. The resulting interaction energy is given by

$$\Delta E_{\mathrm{B}}(\epsilon) = -\sum_{i \text{ in } S} \int \mathbf{F}_i^{\dagger} \cdot \mathrm{d}\mathbf{R}_i \approx -\sum_{i \text{ in } S} \mathbf{F}_i^{\ddagger} \cdot \Delta R_i$$

where $\Delta E_{\mathrm{B}}(\epsilon)$ is the binding energy change due to strain $\epsilon$, $\mathbf{F}_i^{\dagger}$ is the eigenforce vector on a surface atom $i$ induced by relaxing the adsorbate on a geometry-fixed unstrained surface cell, and $\mathrm{d}R_i$ is the displacement vector of the corresponding atom due to the external strain, as depicted in Figure 8a. In the fully rigorous form, $\mathbf{F}_i^{\dagger}$ is a function of the displacement; for simplicity here we assume it to be a constant (denoted $\mathbf{F}_i^{\ddagger}$), resulting in the simplified form to the right. We refer to this as the simplified eigenforce model; this model also ignores surface relaxation effects. Although a more rigorous form could, for example, allow the forces to vary harmonically, as we will show, we can achieve a reasonably quantitative prediction with just the simple approach. In the equation, we only perform DFT calculations to obtain the eigenforces $\mathbf{F}_i^{\ddagger}$, whereas the displacement vector is a simple linear function of the external strain. Thus, it simplifies the pure strain effect to calculate the eigenforces on an unstrained surface cell, without any additional DFT calculations on the strained systems. For more details on the eigenforce model, we refer the readers to our previous works.[18,19]

We apply the eigenforce model to predict the strain susceptibilities of 9 $AH_x$ (A = O, N, and C) molecular fragments at their most preferred adsorption sites on Cu, Pd, and Pt surfaces. We compare the strain susceptibilities obtained by the electronic structure calculator (DFT) to the model predictions. The results are shown in Figure 8b. We see that this simple model can capture the trends in the susceptibility quite well; the MAE across diverse adsorption systems is 0.013 eV/%. Figure 8b shows that the eigenforce predictions tend to overestimate the DFT-calculated values, in particular for $CH_x$ adsorbates on the Pt(111) surface. When one uses the simplified eigenforce model, the prediction deviations mainly originate from three effects, including the variation of eigenforces with strain, strain-induced surface relaxations, and changes of hybridization states within multiatom adsorbates due to strain. Using the outlier example of CH at an fcc site of Pt, we found that the bond length between C and H remains almost constant, irrespective of strains, hence excluding the third effect. Moreover, usually the variation of eigenforces cancels out for strain susceptibilities. Therefore, the large prediction error is mainly attributed to unaccounted surface relaxations. To further confirm the surface relaxation as the main error origin for Pt, in Figure 8c and Figure S6, we compared the eigenforce predictions to the DFT results for rigid systems, excluding the influences of surface relaxations. The overall MAE for unrelaxed systems decreased to 0.009 eV/%. Also, the prediction MAE for Pt went down significantly from 0.024 to 0.009 eV/%. Trends of material, adsorbate, and site dependencies represented by the model predictions are also consistent with DFT calculations.

## 4. CONCLUSIONS

We have presented a systematic study, based on a large set of electronic structure calculations, of the susceptibilities of materials, adsorption sites, and adsorbates to in-plane biaxial strain. DFT calculations were performed on a series of $AH_x$ (A = O, N, and C) molecular fragments on fcc(111) facets of the common late-transition metals of significance to catalysis. The strain susceptibility was quantified as the slope of plots of adsorption energies versus strain within a narrow range of ±2.0% strain. This uncovered certain trends on these (111) surfaces:

1. Pt is most affected by strain, followed by Pd and Au, then finally Ag and Cu. This correlates with the response of the d-band width to strain. The d-band width susceptibility is proportional to the susceptibility of d−d coupling matrix element to strain, which, based on the tight-binding model, can be simply evaluated as a function of the extent of d orbitals and lattice constants (see Figure 4).
2. Threefold binding sites are typically more susceptible to strain than twofold sites, and twofold sites are more susceptible than ontop sites. That is, sites with higher coordination numbers exhibit higher susceptibilities (see Figure 5).
3. Adsorbates having the larger valency tend to display higher susceptibilities to strain, and among adsorbates of the same valency, N-centered adsorbates exhibit similar susceptibilities compared to O-centered adsorbates, while both adsorbates show stronger responsiveness to strain than C-centered adsorbates (see Figure 6).


https://doi.org/10.1021/acs.jpcc.2c07246
J. Phys. Chem. C 2022, 126, 20892−20902

4. A unique scaling relation induced by strain is identified and can cause a departure from known scaling relations, and a simple analysis using coordination numbers is proposed to explain the observation (see Figure 7).
5. Moreover, a mechanical model is used to rationalize the strain trends for diverse model systems. The model predictions are in good agreement with values by electron structure calculations. The eigenforce model offers a simple and unique approach to predict the pure strain effect for a specific adsorbate−surface-site combination, without performing additional calculations on strained systems (see Figure 8).

## ■ ASSOCIATED CONTENT

### Supporting Information

The Supporting Information is available free of charge at https://pubs.acs.org/doi/10.1021/acs.jpcc.2c07246.

Correlation between $d\bar{\varepsilon}_d/de_{x,y}$ and $dW_d/de_{x,y}$; derivation of the susceptibility of d−d coupling matrix element to an equi-biaxial strain; eigenforce analysis for an outlier of site dependency; scaling relationships of $OH_x$ vs O and $CH_x$ vs C; and detailed comparisons between eigenforce-predicted susceptibilities with DFT values (PDF)

## ■ AUTHOR INFORMATION


### Corresponding Author

**Andrew A. Peterson** − *School of Engineering, Brown University, Providence, Rhode Island 02912, United States;* orcid.org/0000-0003-2855-9482; Phone: +1 401-863-2153; Email: andrew_peterson@brown.edu

### Authors

**Cheng Zeng** − *School of Engineering, Brown University, Providence, Rhode Island 02912, United States*

**Tuhina Adit Maark** − *School of Engineering, Brown University, Providence, Rhode Island 02912, United States;* Present Address: Department of Physics, Indian Institute of Technology Madras, Chennai 600036, India

Complete contact information is available at: https://pubs.acs.org/10.1021/acs.jpcc.2c07246


### Author Contributions

‡C.Z. and T.A.M. contributed equally to this work.

### Author Contributions

T.A.M. and A.A.P. designed the work. C.Z. and T.A.M. performed all of the calculations. C.Z., T.A.M., and A.A.P analyzed the data and wrote the paper. T.A.M. observed the correlation between the strain susceptibility of binding energies and susceptibility of d-band width. C.Z. derived the expression for coupling matrix element susceptibility to strain based on the tight-binding model. C.Z. performed the eigenforce model analysis.

### Notes

The authors declare no competing financial interest.

## ■ ACKNOWLEDGMENTS

This material is based upon work supported by the U.S. Army Research Laboratory and the U.S. Army Research Office under the Multi University Research Initiative MURI grant number W911NF-11-1-0353 at Brown University. The authors thank William Curtin, Michael Francis, Pradeep Guduru, and Alireza Khorshidi for fruitful discussions. Cheng Zeng gratefully acknowledges the support from the Presidential Fellowship at Brown University. Electronic structure calculations were carried out at the Brown University Center for Computation and Visualization (CCV).

## ■ REFERENCES


(1) Zhang, J.; Vukmirovic, M. B.; Xu, Y.; Mavrikakis, M.; Adzic, R. R. Controlling the catalytic activity of platinum-monolayer electrocatalysts for oxygen reduction with different substrates. *Angew. Chem., Int. Ed.* **2005**, *44*, 2132−2135.

(2) Kibler, L. A.; El-Aziz, A. M.; Hoyer, R.; Kolb, D. M. Tuning reaction rates by lateral strain in a palladium monoloayer. *Angew. Chem., Int. Ed.* **2005**, *44*, 2080−2084.

(3) Chen, M.; Kumar, D.; Yi, C. W.; Goodman, D. W. The promotional effect of gold in catalysis by palladium-gold. *Science* **2005**, *310*, 291−293.

(4) Pallassana, V.; Neurock, M. Electronic factors governing ethylene hydrogenation and dehydrogenation activity of pseudomorphic PdML/Re(0001), PdML/Ru(0001), Pd(111), and PdML/Au(111) surfaces. *J. Catal.* **2000**, *191*, 301−317.

(5) Baddeley, C. J.; Ormerod, R. M.; Stephenson, A. W.; Lambert, R. M. Surface structure and reactivity in the cyclization of acetylene to benzene with Pd overlayers and Pd/Au surface alloys on Au(111). *J. Phys. Chem. A* **1995**, *99*, 5146−5151.

(6) Greeley, J.; Nørskov, J. K.; Kibler, L. A.; El-Aziz, A. M.; Kolb, D. M. Hydrogen evolution over bimetallic systems: understanding the trends. *ChemPhysChem* **2006**, *7*, 1032−1035.

(7) Hammer, B.; Nørskov, J. K. Electronic factors determining the reactivity of metal surfaces. *Surf. Sci.* **1995**, *343*, 211−220.

(8) Hammer, B.; Morikawa, Y.; Nørskov, J. K. CO chemisorption at metal surfaces and overlayers. *Phys. Rev. Lett.* **1996**, *76*, 2141−2144.

(9) Ruban, A.; Hammer, B.; Stoltze, P.; Skriver, H. L.; Nørskov, J. K. Surface electronic structure and reactivity of transition and noble metals. *J. Mol. Catal. A* **1997**, *115*, 421−429.

(10) Adit Maark, T.; Peterson, A. A. Understanding strain and ligand effects in hydrogen evoltuion over Pd(111) surfaces. *J. Phys. Chem. C* **2014**, *118*, 4275−4281.

(11) Rodriguez, J. A.; Goodman, D. W. Surface science studies of the electronic and chemical properties of bimetallic systems. *J. Phys. Chem. B* **1991**, *95*, 4196−4206.

(12) Rodriguez, J. A.; Campbell, R. A.; Goodman, D. W. Electronic interactions in bimetallic systems: Core-level binding energy shifts. *J. Vac. Sci. Technol. A* **1991**, *9*, 1698−1702.

(13) Strasser, P.; Koh, S.; Anniyev, T.; Greeley, J.; More, K.; Yu, C.; Liu, Z.; Kaya, S.; Nordlund, D.; Ogasawara, H.; et al. Lattice-strain control of the activity in dealloyed core-shell fuel cell catalysts. *Nat. Chem.* **2010**, *2*, 454−460.

(14) Yang, Y.; Adit Maark, T.; Peterson, A.; Kumar, S. Elastic strain effects on catalysis of a PdCuSi metallic glass thin film. *Phys. Chem. Chem. Phys.* **2015**, *17*, 1746−1754.

(15) Kitchin, J. R.; Nørskov, J. K.; Barteau, M. A.; Chen, J. G. Role of strain and ligand effects in the modification of the electronic and chemical properties of bimetallic surfaces. *Phys. Rev. Lett.* **2004**, *93*, No. 156801.

(16) Kitchin, J. R.; Nørskov, J. K.; Barteau, M. A.; Chen, J. G. Modification of the surface, electronic and chemical properties of Pt(111) by subsurface 3d transition metals. *J. Chem. Phys.* **2004**, *120*, 10240−10246.

(17) Khorshidi, A.; Violet, J.; Hashemi, J.; Peterson, A. A. How strain can break the scaling relations of catalysis. *Nat. Catal.* **2018**, *1*, 263−268.

(18) Sharma, S.; Zeng, C.; Peterson, A. A. Face-centered tetragonal (FCT) Fe and Co alloys of Pt as catalysts for the oxygen reduction reaction (ORR): A DFT study. *J. Chem. Phys.* **2019**, *150*, No. 041704.

(19) Li, J.; Sharma, S.; Wei, K.; Chen, Z.; Morris, D.; Lin, H.; Zeng, C.; Chi, M.; Yin, Z.; Muzzio, M.; et al. Anisotropic strain tuning of

L10 ternary nanoparticles for oxygen reduction. *J. Am. Chem. Soc.* **2020**, *142*, 19209−19216.
(20) Sun, X.; Li, D.; Ding, Y.; Zhu, W.; Guo, S.; Wang, Z. L.; Sun, S. Core/shell Au/CuPt nanoparticles and their dual electrocatalysis for both reduction and oxidation reactions. *J. Am. Chem. Soc* **2014**, *136*, 5745−5749.
(21) Yan, K.; Maark, T. A.; Khorshidi, A.; Sethuraman, V. A.; Peterson, A. A.; Guduru, P. R. The influence of elastic strain on catalytic activity in the hydrogen evolution reaction. *Angew. Chem., Int. Ed.* **2016**, *55*, 6175−6181.
(22) Yan, K.; Kim, S. K.; Khorshidi, A.; Guduru, P. R.; Peterson, A. A. High elastic strain directly tunes the hydrogen evolution reaction on tungsten carbide. *J. Phys. Chem. C* **2017**, *121*, 6177−6183.
(23) Deng, Q.; Smetaninb, M.; Weissmüller, J. Mechanical modulation of reaction rates in electrocatalysis. *J. Catal.* **2014**, *309*, 351−361.
(24) Johnson, B.; Guduru, P. R.; Peterson, A. A. Strain-induced changes to the methanation reaction on thin-film nickel catalysts. *Catal. Sci. Technol.* **2019**, *9*, 3279−3286.
(25) Tsevtkov, N.; Lu, Q.; Chen, Y.; Yildiz, B. Accelerated oxygen exchange kinetics of Nd2NiO(4+$\delta$) thin films with tensile strain long c-axis. *ACS Nano* **2015**, *9*, 1613−1621.
(26) Yildiz, B. "Stretching" the energy landscape of oxides—Effects on electrocatalysis and diffusion. *MRS Bull.* **2014**, *39*, 147−156.
(27) Mavrikakis, M.; Hammer, B.; Nørskov, J. K. Effect of strain on the reactivity of metal surfaces. *Phys. Rev. Lett.* **1998**, *81*, 2819−2822.
(28) Xu, Y.; Mavrikakis, M. Adsorption and dissociation of O2 on Cu(111): Thermochemistry, reaction Barrier and the effect of strain. *Surf. Sci.* **2001**, *494*, 131−144.
(29) Xu, Y.; Mavrikakis, M. Adsorption and dissociation of O2 on gold surfaces: Effect of steps and strain. *J. Phys. Chem. B* **2003**, *107*, 9298−9307.
(30) Sakong, S.; Groß, A. Dissociative adsorption of hydrogen on strained Cu surfaces. *Surf. Sci.* **2003**, *525*, 107−118.
(31) Voiry, D.; Yamaguchi, H.; Li, J.; Silva, R.; Alves, D. C. B.; Fujita, T.; Chen, M.; Asefa, T.; Shenoy, V. B.; Eda, G.; Chhowalla, M. Enhanced catalytic activity in strained chemically exfoliated WS2 nanosheets for hydrogen evolution. *Nat. Mat.* **2013**, *12*, 850−855.
(32) Abild-Pedersen, F.; Greeley, J.; Studt, F.; Rossmeisl, J.; Munter, T. R.; Moses, P. G.; Skulason, E.; Bligaard, T.; Nørskov, J. K. Scaling properties of adsorption energies for hydrogen-containing molecules on transition-metal surfaces. *Phys. Rev. Lett.* **2007**, *99*, No. 016105.
(33) Nørskov, J. K.; Rossmeisl, J.; Logadottir, A.; Lindqvist, L.; Kitchin, J. R.; Bligaard, T.; Jonsson, H. Origin of overpotential for oxygen reduction reaction at a fuel-cell cathode. *J. Phys. Chem. B* **2004**, *208*, 17886−17892.
(34) Karlberg, G. S.; Rossmeisl, J.; Nørskov, J. K. Estimations of electric field on the oxygen reduction reaction based on density functional theory. *Phys. Chem. Chem. Phys.* **2007**, *9*, 5158−5161.
(35) Viswanathan, V.; Hansen, H. A.; Rossmeisl, J.; Norskov, J. K. Unifying the 2e− and 4e− reduction of oxygen on metal surfaces. *J. Phys. Chem. Lett.* **2012**, *3*, 2948−2951.
(36) Hansen, H. A.; Varley, J. B.; Peterson, A. A.; Nørskov, J. K. Understanding trends in the electrocatalytic activity of metals and enzymes for $CO_2$ reduction to CO. *J. Phys. Chem. Lett.* **2013**, *4*, 388−392.
(37) Peterson, A. A.; Nørskov, J. K. Activity descriptors for CO2 electroreduction to methane on transition-metal catalysts. *J. Phys. Chem. Lett.* **2012**, *3*, 251−258.
(38) Jones, G.; Bligaard, T.; Abild-Pedersen, F.; Nørskov, J. K. Using scaling relations to understand trends in the catalytic activity of transition metals. *J. Phys.: Condens. Matter.* **2008**, *20*, No. 064239.
(39) Mortensen, J. J.; Hansen, L. B.; Jacobsen, K. W. Real-space grid implementation of the projector augmented wave method. *Phys. Rev. B* **2005**, *71*, No. 035109.
(40) Enkovaara, J.; Rostgaard, C.; Mortensen, J. J.; Chen, J.; Dułak, M.; Ferrighi, L.; Gavnholt, J.; Glinsvad, C.; Haikola, V.; Hansen, H. A.; et al. Electronic structure calculations with GPAW: a real-space implementation of the projector augmented-wave method. *J. Phys.: Condens. Matter* **2010**, *22*, No. 253202.
(41) Larsen, A.; Mortensen, J.; Blomqvist, J.; Castelli, I.; Christensen, R.; Dulak, M.; Friis, J.; Groves, M.; Hammer, B.; Hargus, C.; et al. The atomic simulation environment - A python library for working with atoms. *J. Phys.: Condens. Matter* **2017**, No. 273002.
(42) Hammer, B.; Hansen, L. B.; Nørskov, J. K. Improved adsorption energetics within density-functional theory using revised Perdew-Burke-Ernzerhof functionals. *Phys. Rev. B* **1999**, *59*, 7413−7421.
(43) Wellendorff, J.; Silbaugh, T. L.; Garcia-Pintos, D.; Nørskov, J. K.; Bligaard, T.; Studt, F.; Campbell, C. T. A benchmark database for adsorption bond energies to transition metal surfaces and comparison to selected DFT functionals. *Surf. Sci.* **2015**, *640*, 36−44.
(44) Peterson, A. A.; Grabow, L. C.; Brennan, T. P.; Shong, B.; Ooi, C.; Wu, D. M.; Li, C. W.; Kushwaha, A.; Medford, A. J.; Mbuga, F.; Li, L.; Nørskov, J. K. Finite-size effects in O and CO adsorption for the late transition metals. *Top. Catal.* **2012**, *55*, 1276−1282.
(45) Harrison, W. A. *Electronic Structure and the Properties of Solids: The Physics of the Chemical Bond*; W H Freeman & Co., 1980.
(46) Nørskov, J. K. et al. *Fundamental Concepts in Heterogeneous Catalysis*; John Wiley & Sons, Ltd., 2014; pp 175−194.
(47) Pauling, L. The nature of the chemical bond. IV. The energy of single bonds and the relative electronegativity of atoms. *J. Am. Chem. Soc.* **1932**, *54*, 3570−3582.
(48) Allred, A. L. Electronegativity values from thermochemical data. *J. Inorg. Nucl. Chem.* **1961**, *17*, 215−221.
(49) Blokker, E.; Sun, X.; Poater, J.; van der Schuur, J. M.; Hamlin, T. A.; Bickelhaupt, F. M. The chemical bond: When atom size instead of electronegativity difference determines trend in bond strength. *Chem. - Eur. J.* **2021**, *27*, 15616−15622.
(50) Albright, T. A.; Burdett, J. K.; Whangbo, M.-H. *Orbital Interactions in Chemistry*; John Wiley & Sons, 2013.
(51) Montemore, M. M.; Medlin, J. W. Scaling relations between adsorption energies for computational screening and design of catalysts. *Catal. Sci. Technol.* **2014**, *4*, 3748−3761.
(52) Xin, H.; Linic, S. Communications: Exceptions to the d-band model of chemisorption on metal surfaces: The dominant role of repulsion between adsorbate states and metal d-states. *J. Chem. Phys.* **2010**, *132*, No. 221101.
(53) Montemore, M. M.; Medlin, J. W. Site-specific scaling relations for hydrocarbon adsorption on hexagonal transition metal surfaces. *J. Phys. Chem. C* **2013**, *117*, 20078−20088.
(54) Bhattacharjee, S.; Waghmare, U. V.; Lee, S.-C. An improved d-band model of the catalytic activity of magnetic transition metal surfaces. *Sci. Rep.* **2016**, *6*, No. 35916.


https://doi.org/10.1021/acs.jpcc.2c07246
J. Phys. Chem. C 2022, 126, 20892−20902